Rapalink-1 reveals novel mTOR-dependent genes and the role of agmatinases in cellular growth and chronological lifespan

Juhi Kumar[1] and Charalampos Rallis[1,*]

[1]Research Centre for Molecular Cell Biology, School of Biological and Behavioural Sciences, Queen Mary, University of London, Mile End Road, London E1 4NS, UK.

[*]Author for correspondence: c.rallis@qmul.ac.uk

Abstract

mTOR is a conserved pro-ageing pathway with characterised inhibitors such as rapamycin, rapalogues and torins. A third-generation inhibitor, rapalink-1, has been developed, however, its effects on organismal gene expression and lifespan have not been evaluated. Here, we demonstrate that rapalink-1 affects fission yeast spatial and temporal growth and prolongs chronological lifespan. Endosome and vesicle-mediated transport and homeostasis processes related to autophagy and Pik3, the orthologue of human PI3K, render cells resistant to rapalink-1. Our study reveals mTOR-regulated genes with unknown roles in ageing including all fission yeast agmatinases, the enzymes responsible for processing agmatine to putrescine and urea. We identify sensitive and resistant mutants to agmatine and putrescine and show that all fission yeast agmatinase enzymes are required for normal lifespan. Genetic interactome assays for the agmatinase *agm1* and further cell and molecular analyses, demonstrate that impairing the agmatinergic branch of arginine catabolism results in mTOR activity levels that are beneficial for growth but detrimental for chronological ageing. Our study reveals metabolic feedback circuits with possible implications to other systems, including human cells.

Key words: Ageing, mTORC1, mTORC2, agmatine, putrescine, polyamines, rapamycin, torin1, nutrient response, *S. pombe*, MLN0128, sapanisertib

Introduction

Pharmacological inhibition of the evolutionarily conserved, nutrient-responsive and pro-ageing mechanistic Target of Rapamycin signalling pathway presents great interest in disease and biogerontology

(Bjedov and Partridge, 2011; Laplante and Sabatini, 2012). The centrepieces of the pathway are the mTOR PI3-related kinases that operate within two structurally and functionally distinct protein complexes, TORC1 and TORC2. The complexes are reported to have roles in both spatial and temporal aspects of cellular growth (Ikai et al., 2011). While TORC1 is responsible for promoting protein translation, lipid and central carbon metabolism and inhibiting autophagy, TORC2 regulates cytoskeleton and is required for cell survival (Bjedov and Rallis, 2020; Gonzalez and Rallis, 2017; Ikai et al., 2011). Rapamycin, a macrolide able to inhibit TORC1 in an allosteric manner through interaction with the FKBP12 protein (Fkh1 in fission yeast), is shown to extend lifespan in cellular and animal models (Bjedov and Partridge, 2011; Harrison et al., 2009; Rallis et al., 2017, 2013). Torin1, a dual ATP-competitive inhibitor of TORC1 and TORC2 has also been shown to be beneficial for lifespan in various models including fission yeast (Rodríguez-López et al., 2020). Both drugs together with several rapalogues are used in numerous clinical trials (www.clinicaltrials.org).

Rapalink-1 is a third generation mTOR inhibitor that combines rapamycin and sapanisertib (MLN0128) (Fan et al., 2017). Its structure does not disrupt the binding of rapamycin to FKBP12 or the FRB domain of mTOR. While MLN0128 has been shown to have poor *in vivo* efficacy, its link to rapamycin has shown great promise in targeted TORC1 inhibition and cancer regression (Fan et al., 2017; Kuroshima et al., 2020). Rapalink-1 has been reported to prevent ethanol-induced senescence in endothelial cells (Zhou et al., 2023). Nevertheless, its precise effects on chronological lifespan have not been addressed.

Here, we have investigated the effects of rapalink-1 through comparisons with rapamycin using fission yeast, a relevant model in cell biology and ageing studies (Legon and Rallis, 2022; Roux et al., 2010, 2009). Both drugs advance mitosis in fission yeast without halting the cell cycle like the pan-mTOR inhibitor torin1 (Rodríguez-López et al., 2020) and can prolong chronological lifespan. The effects observed on gene expression following rapalink-1 treatment, are consistent with TORC1 inhibition (Petersen and Nurse, 2007; Rallis et al., 2017, 2013; Rodríguez-López et al., 2020). Using a combination of classical cell biology and genome-wide cell-based screens we uncover new mTOR-related genes and demonstrate that the enzymes converting agmatine to urea and the polyamine putrescine (agmatinases) are a pivotal pathway that impacts lifespan. Analysis of genetic interactome of agmatinase *agm1* (Lock et al., 2020; Rutherford et al., 2024) together with cellular and molecular analyses, uncover a metabolic regulatory feedback loop that impacts on mTOR activity itself and with possible implications to other organisms, including human cells.

Results

Rapalink-1 affects cell cycle progression, cell size and TORC1-dependent processes in fission yeast.

Rapalink-1 is reported to inhibit mTORC1 (Fan et al., 2017; Kuroshima et al., 2020). We, therefore, wished to investigate its effects through comparing it with rapamycin, a well-characterised and widely used TORC1 inhibitor and without the complications of dual (TORC1 and TORC2) inhibitors such as torin1 (Thoreen et al., 2009; Thoreen and Sabatini, 2009). Rapamycin-induced inhibition of mTOR advances mitotic onset, mimicking the reduction in cell size at division observed following shifts to poor nitrogen sources (Petersen and Nurse, 2007). We, therefore, analysed related effects when cells are treated with 100nM rapamycin and rapalink-1 as this concentration of rapamycin has been shown previously to inhibit TORC1-related processes in fission yeast, (Rallis et al., 2017, 2013). In rich YES media, treatment with rapamycin and rapalink-1 leads to increased mitotic index (49% and 37% respectively compared to 27% in control cells), peaking at 30-minute post treatments (Figure 1A). Similarly, when cells are treated with rapamycin in EMM2 the mitotic index peaks at 30 minutes post-treatment (44% compared to 20% in control cells) returning to levels comparable with the untreated cells following this (Figure 1B). Treatment with rapalink-1 leads to a milder but sustained increase in the mitotic index (27%, 26% and 32% at 30’, 60’ and 120’ respectively). Along with mitotic onset, treatments with both rapamycin and rapalink-1 result in decreased cell size upon division in rich YES media (see 30’-120’ time course in Figure 1C). Rapamycin has a more severe effect on cell size compared to rapalink-1, at least in these media (Figure 1C) with gradual decrease over time (from 30 to 120 minutes) while cells following rapalink-1 treatment decrease their size in 30 minutes and remain in the same levels for the whole examined period of two hours (Figure 1C). Likewise, in minimal EMM2 media, cell sizes upon division decrease for both rapamycin and rapalink-1 (Figure 1D). The patterns of cell sizes differ between the two drugs: while in rapamycin cells reach their minimum size in 60 minutes (12.4 μm) and then start to gradually recover, in rapalink-1 they decrease in 90 minutes (13.5 μm) and remain at the same size range for the duration (120’) of the assay (Figure 1D).

Our septation and cell size results indicate phenotypes related to TORC1 inhibition as previously shown and described (Petersen and Nurse, 2007; Rallis et al., 2017, 2013; Rodríguez-López et al., 2020). We, therefore, investigated whether drug treatments at these concentrations affect multiple aspects of TORC1 functions (Gonzalez and Rallis, 2017). Negative cross-regulation between the AMPK and TORC1 pathways have been previously reported in fission yeast (Davie et al., 2015; Ling et al., 2020). We, therefore,

examined the phosphorylation status of the fission yeast serine/threonine protein kinase AMPK catalytic (alpha) subunit Ssp2. Following two and five hours of treatment with 100nM of rapamycin or rapalink-1, no observable changes in Ssp2 phosphorylation are found (Figure 1E). TORC1 negatively regulates autophagy (Gonzalez and Rallis, 2017). Examination of GFP-Atg8 patterns (Mukaiyama et al., 2010) following drug treatment in the aforementioned time points, do not show a significant degree of processing (Mukaiyama et al., 2010) indicating that autophagy may not be upregulated or that it may be upregulated (albeit only marginally) in these conditions (Figure 1E). Contrary to autophagy, global protein translation might be suppressed five hours post-treatment with both drugs, as seen through phosphorylation of eIF2α while its total levels remain unchanged at both two-hour and five-hour time points examined. Finally, we wondered whether drug treatment can affect the activity of Maf1, a Pol III repressor (Noguchi et al., 2021), through its TORC1-dependent phosphorylation status (Davie et al., 2015). Immunoblotting for Maf1-pK revealed that following treatment with both rapamycin and rapalink-1, Maf1-pK becomes dephosphorylated, more evidently in five hours of treatment (Figure 1E).

We have, previously, shown that the GATA transcription factor Gaf1 mediates Pol II- and Pol III-mediated transcription downstream of TORC1 (Rodríguez-López et al., 2020). Gaf1 is localised mainly in the cytoplasm and upon TORC1 inhibition translocates to the nucleus and binds target genes (Rodríguez-López et al., 2020). We examined localisation of Gaf1-GFP (controlled by the endogenous Gaf1 promoter as described in Rodríguez-López et al., 2020). Gaf1-GFP signal is found throughout the cell in untreated cells (Figure 1F). Treatment with rapamycin and rapalink-1 results in nuclear localization of Gaf1-GFP within 5 minutes (Figure 1F) indicating that both drugs can inhibit TORC1 at sufficient levels to allow Gaf1 dephosphorylation and translocation. One of the major actions of Gaf1 is to repress all the Pol III transcribed tRNAs in fission yeast upon TORC1 inhibition. The result of Gaf1-GFP localisation agrees with Maf1 activation seen through Maf1-pK dephosphorylation (Figure 1E). Overall, our results show that rapalink-1 targets fission yeast TORC1 and, like rapamycin, can inhibit several but not all aspects of TORC1-dependent functions in the examined concentrations.

We then assessed the chronological lifespan (CLS) of fission yeast cells when treated with rapamycin and rapalink-1 in YES media and at OD_{600} 0.5 at 100nM concentration. As expected, rapamycin induces CLS extension (Fig.1G, log-rank $p=1.25*10^{-12}$). Similarly, rapalink-1 prolongs lifespan in similar fashion to rapamycin (Fig.1H, $p=2.2*10^{-12}$) demonstrating the potential of the drug and its action in ageing

through TORC1 inhibition. Rapalink-1 lifespan extension depends on *fkh1* (Fig. 1H, p=0.047) as has previously been observed in the case of rapamycin (Rallis et al., 2013) demonstrating that the effects of rapalink-1 in these conditions are TORC1-dependent.

A genome-wide screen for rapalink-1 resistance highlights roles of endosome-related processes in growth and lifespan

Previous data in fission yeast have shown that mTOR inhibition results in lifespan extension with (in the case of torin1) or without (in the case of rapamycin) cell-cycle progress inhibition. Fast growing cultures of wild-type fission yeast cells at OD_{600} 0.2 were treated either with DMSO (control) or rapamycin and rapalink-1 at a 100nM concentration. Cultures were placed at a Biolector setup as previously described (Rallis et al., 2013) and growth was monitored continuously through light scattering measurements (Rallis et al., 2017, 2014, 2013). While no lag phase following drug treatment is observed (Figure 2A), a mild growth effect is seen in this assay consistent with results previously seen with rapamycin (Rallis et al., 2013). We then performed a genome-wide fitness screen for rapalink-1 using the Bioneer deletion library (Kim et al., 2010) at two rapalink-1 concentrations (100 nM and 300 nM, Figure 2B) and at conditions that each mutant is assessed and measured in quadruplicate (Rallis et al., 2017; Rodríguez-López et al., 2020). Results from the screens correlate well (Pearson cor.coeff=0.73, Figure 2C, supplemental table 1). Sensitive strains are related to protein translation, sulphur metabolism and mitochondrial membrane organisation among others (Figure 2D) representing proteins and groups related to anabolic functions and cellular growth (Laxman et al., 2013). Resistant strains are related to CAMKK-AMPK signalling, vacuole and vesicle-mediated transport and autophagy (Figure 2E). The fitness signatures acquired are consistent with TORC1 inhibition with GO groups functionally linked to transport of macromolecules, processing of proteins, membranes and autophagic functions (Figure 2F) representing fundamental metabolic functions in the crossroads of catabolism and growth (Gilleron et al., 2019). Most of these mutants are required for normal lifespan (Romila et al., 2021) and they have been identified in previous mTOR inhibition screens from our group (Rodríguez-López et al., 2020) and others (Lie et al., 2018). We wondered whether such factors are required for rapalink-1-dependent lifespan extension. We have, therefore, performed CLS analysis for the related *pik3* mutant as a proof of principle. *Pik3Δ* cells are short-lived compared to *wt* (Figure 2G, compare with Figure 1H) demonstrating that it is required for normal chronological lifespan in fission yeast. Nevertheless,

rapalink-1 prolongs lifespan of *pik3* mutant cells (log rank, $p=10^{-5}$). To quantify the role of Pik3 in rapalink-1-mediated longevity and directly compare with the rapalink-1 effects on *wt* cells, we calculated the areas under the curve (AUCs, measured as days × percentage of survival from lifespan assays). In wild-type cells, the lifespan was prolonged from an average AUC of 692 to 2,351 (increase of 1,659), whereas in *pik3Δ* cells, the lifespan was prolonged to a lesser extent, from an average AUC of 473 to 1431 (increase of 958) (Figure 2H). A major difference between the rapalink-1 lifespan increase between normal and *pik3Δ* mutant cells is in the first day of CLS: rapalink-1 can prolong the healthspan of *wt* in this timeframe (cell population retains viability close to 100%, Figure 1H).

Rapalink-1-dependent gene expression points to TORC1-related genes with both known and unknown roles in ageing

Beyond proteostasis, autophagy and global translation levels, TORC1 activity controls gene expression at the level of transcription through multiple transcription factors (Bjedov and Rallis, 2020; Rodríguez-López et al., 2023; Schmeisser and Parker, 2019). We therefore performed RNA-seq analysis on fission yeast cells treated with 100nM rapamycin and rapalink-1 for 5 hrs. This timepoint was chosen based on the observed changes in the relevant markers described at Figure 1E.

PCA analysis shows that Rapalink-1 induces a stronger effect on gene expression compared to rapamycin with the PCA1 component accounting for 71.36% difference between control, rapamycin and rapalink-1 datasets separating well rapalink-1-treated transcriptomes from untreated and rapamycin-treated states (Figure 3A). In these conditions, 17 genes are 2-fold, 70 genes 1.5-fold and 277 genes 1.2-fold upregulated in rapamycin-treated cells compared to untreated cells while 2, 4 and 87 genes are downregulated at the 2-fold, 1.5-fold and 1.2-fold levels respectively (Figure S1A, supplemental tables 2 and 3). In the case of Rapalink-1-treated cells, 190 genes are 2-fold, 355 genes 1.5-fold and 701 genes 1.2-fold upregulated while 4, 28 and 516 are downregulated (Figure S1B) compared to untreated cells (see supplemental tables 4 and 5). Interestingly, our analyses reveal 277 genes upregulated and 87 downregulated genes in rapalink-1 compared to rapamycin (Figure S1C). Following rapamycin treatment, the downregulated gene list is enriched among others in cytoplasmic translation, tRNA metabolic process and transcription by polymerase III (Figure 2B). Upregulated genes are involved in cell cycle and specifically in mitotic prometaphase. On the other hand, the gene list of rapalink-1-upregulated genes are enriched in

vacuolar transport and organisation. This has been previously observed in the case of torin1-treated fission yeast cells ((Rodríguez-López et al., 2020). The subcellular localisation of TORC1 in fission yeast (Valbuena et al., 2012a) is predominantly on the vacuole. It is interesting that factors related to biogenesis and dynamics of the organelle where mTORC1 resides on, transcriptionally depend on mTORC1 activity. In addition, small molecule, amino acid metabolic processes and transmembrane transport are also enriched categories, among others (Figure 2B). While both rapamycin and rapalink-1 target TORC1 and modulate lifespan in a similar fashion (in terms of lifespan extension patterns), it may be that they do so through the regulation of common as well as distinct genes, at least, in the given analysed conditions. We, therefore, examined the overlaps of upregulated and downregulated genes for the two drugs as well as genes that are apparently regulated differently between the two pharmacological treatments. 541 upregulated (Figure 2C) and 475 downregulated (Figure 2D) genes are unique to rapalink-1. Genes that are upregulated in rapalink-1 compared to rapamycin are related to small molecule catabolic processes, arginine and proline metabolism, glycolysis, transmembrane transport and small molecule catabolic processes (just to name a few, see Figure S1D) while downregulated genes are related to ribosome biogenesis, translation, amino acid and tRNA metabolic processes (Figure S1E).

High-throughput phenotyping approaches have majorly contributed to characterising the chronological lifespan of haploid fission yeast mutants (Rodríguez-López et al., 2023; Romila et al., 2021). TORC1 is a major pro-ageing pathway and TORC1-dependent genes are likely to be related in lifespan regulation. We, therefore, examined whether differentially expressed genes from rapalink-1-treated cells are linked with long or short reported lifespans of the corresponding mutants. While many rapalink-1 upregulated genes have reported lifespans, a significant number (331 genes) have no lifespan annotations (Figure 3E). GO enrichment of these genes demonstrates that they are related to amino acid transport, amide transport, galactose, tyrosine arginine and proline metabolism (Figure S2A). Likewise, 150 genes that are found to be downregulated in rapalink-1 treated cells have not been annotated for lifespan (Figure S2B) and these are related to L13a-mediated translational silencing, ribonucleoside biosynthesis, response to stimulus as well as to alanine, aspartate and glutamate metabolism (Figure S2C). Examination of upregulated genes not linked yet to lifespan, revealed that arginine catabolism and specifically all the agmatinase enzymes involved in processing agmatine to putrescine are boosted following TORC1 inhibition (Figure 3F). We therefore wondered whether agmatinases are required for normal chronological lifespan. CLS assays reveal

that *agm1Δ* (log rank p=9.7x10^{-5}, Figure 3G), *agm2Δ* (log rank p=1.5x10^{-5}, Figure 3H) and *agm3Δ* (log rank, p=3.9x10^{-5}, Figure 3I) mutant cells are shortlived compared to wild-type cells. In addition, cells mutant for both *agm1* and *agm3* are also short-lived (log rank p=3.3x10^{-6}, Figure 3J).

Agmatine and putrescine affect growth, metabolism and lifespan

The requirement of agmatinases in normal chronological lifespan led us to wonder about the effects of supplementing agmatine and putrescine on the fitness and lifespan of fission yeast cells. Towards this, we have performed genome-wide screens for both agmatine and putrescine in concentrations that are not toxic and only induce a very small delay in growth (15mM agmatine and 25mM putrescine, data not shown). Each mutant has been assessed in quadruplicate and fitness ratios have been obtained through normalisations with untreated copies of the deletion library (Hayles et al., 2013; Kim et al., 2010). Good quality data have been obtained for 3,208 mutants (Figure 4A). Fitness ratios of the mutant strains between the two screens are well correlated (Pearson cor.coeff=0.74, Figure 4B) showcasing that they have similar metabolic and growth outcomes. Gene ontology enrichments for sensitive and resistant strains (cutoffs set at >1.35 and <0.65 fitness ratios for resistant and sensitive, respectively) show overlapping and unique enrichments (Figure 4C, Supplemental Tables 6 for agmatine and putrescine fitness ratios of all mutants). Both compounds render cells with gene deletions related to arginine metabolism, as sensitive. However, while putrescine affects more strongly ribosome-related mutants, agmatine affects mutants related to cytosolic transport or response to oxygen containing compound (Figure 4C for a complete list of GOs). On the other hand, mutants related to the CAMKK-AMPK signaling cascade (as in the case of rapalink-1) and intracellular transport and tRNA wobble uridine modification are resistant to both agmatine and putrescine. The list of resistant strains to putrescine is enriched in categories related to polyphosphate metabolic process, cellular respiration and chaperone-mediated folding among others (Figure 4C). Interestingly, GO enrichments for strains resistant to agmatine include vacuolar transport and organisation and are reminiscent of lists of mutant strains resistant to rapalink-1 (genes coding for endolysosomal-related proteins). This result together with the requirement of agmatinase enzymes in normal fission yeast chronological lifespan led us to wonder whether agmatine and putrescine supplementation can be beneficial to *S. pombe* CLS. Indeed, addition of both compounds to fast growing wild-type *S. pombe* cultures at the same concentrations used in our genome-wide screens lead to lifespan extension with agmatine having more profound effects (Figure 4D, log rank p=5.3x10^{-11} ; 4E

$p=9.4x10^{-10}$). Our results are consistent with previous observations on the positive effects of agmatine in lifespan and ageing (Pryor et al., 2019). We examined whether agmatinases are required for the lifespan extension and repeated the experiments in the genetic background of *agm1Δ* (Figure 4F, log rank $p=4.4x10^{-13}$; 4G, $p=4.5x10^{-10}$), *agm2Δ* (Figure 4H, log rank $p=3.5x10^{-11}$; 4I, $p=3.5x10^{-8}$) *and agm3Δ* (Figure 4J log rank $p=1.1x10^{-13}$; 4K, $p=2x10^{-9}$), gene deletions. Lifespan extensions comparable with the wild-type cells are observed in all single mutant backgrounds. The same beneficial effects are also observed in double *agm1Δ agm3Δ* mutant cells (Figure 4L log rank $p=4.1x10^{-10}$; 4M, $p=3x10^{-10}$). This might be due to either functional compensation or beneficial effects related to other pathways such as lipid metabolism (Pryor et al., 2019) or through oxidative stress protection (Milosevic et al., 2022).

Agm1 interactome reveals metabolism-mediated mTOR activity regulation with effects on growth and lifespan

To understand the mechanisms underlying the requirements of agmatinases' functions in ageing we performed a Synthetic Genetic Array (SGA) for *agm1* using *ade6::natMX6* as a control SGA query. As the deletion library strains carry *ade6* auxotrophy alleles (Hayles et al., 2013; Kim et al., 2010), the control query/SGA does not affect the fitness profiles of the deletion collection as previously reported in published methods (Rallis et al., 2017). Following normalisations for plate positional effects, low fitness mutants, and linkage we have isolated data for 3,108 double mutants with *agm1* (Supplemental Table 7). Physical mapping of the isolated genetic interactions is reassuring of the successful double mutants' generation as it demonstrates the characteristic accumulation of negative values around the *agm1* locus and the positive values around the control *ade6* locus (Figure 5A). These values have been filtered out during our quality control steps. With interaction value cutoffs of -15 and +15 (see materials and methods) we find 179 mutants to show negative interactions and 284 mutants exhibiting positive interactions with *agm1* (Figure 5B). The negative interaction list is enriched for genes coding for post-transcriptional regulation, carbon metabolism, and reticulophagy among other GO terms (Figure 5C, Supplemental Table 7). Positive interactions are enriched in amide metabolism, stress response and nitrogen metabolism (Figure 5D, Supplemental Table 7).

Close inspection of the interactors' list reveals that genes coding for stress and amino acid sensing that inhibit mTORC1 such as *gcn1* (Valbuena et al., 2012b) and *fil1* (Duncan et al., 2018) positively interact with *agm1* (Figure 5E, green fonts). On the other hand, the mTORC1 core component *tco89* (Ikai et al.,

2011), negatively interacts with *agm1* (Figure 5E, red fonts). These results could mean that absence of *agm1* (and possibly the rest of the agmatinases) promotes growth that is enhanced through the absence of stress response players. The cellular growth enhancement is mTORC1-dependent as absence of *tco89* results in reduced cellular fitness/growth. Therefore, in this scenario, agmatinases may provide a metabolic regulatory feedback for mTORC1 activity in fission yeast: when mTOR is inhibited, cells process vacuole-stored amino acids such as arginine (Mülleder et al., 2016), thus, ensuring that mTOR inhibition signals are maintained, relayed within the cell and preventing anabolism while preparing for catabolic processes and autophagy. In this case, *agm* mutants would showcase phenotypes related to increased mTORC1 activity. Indeed, we have found that all agmatinase deletion mutants have short chronological lifespans compared to *wt* cells (Figure 3G-J). *Agm1* mutants have already been reported to be fast-growing (Sideri et al., 2015) and to have decreased mating efficiency (Dudin et al., 2017), both cellular characteristics of increased mTORC1 activity. We have then assessed cell size upon division for normal (wt) and agmatinase mutants. Our results demonstrate that *agm* mutant cells are larger (Figure 5F, ***: $p<0.001$, Wilcoxon testing) strengthening the case of increased mTORC1 levels as the latter controls both temporal and spatial aspect of fission yeast growth. mTORC1 activity regulates multiple targets related to growth that are mediated through several downstream kinases such as Sck1, Sck2, Psk1 and Gad8. The activity of these downstream of mTOR can be visualised using phospho-Akt target antibody. Although different targets seem to be phosphorylated within the different mutants (Figure 5G) the overall activity seems is enhanced (Figure 5H). Interestingly, while *tco89* mutant cells are long-lived (Rallis et al., 2013), *agm1Δ tco89Δ* are short-lived as single *agm1* mutants (Figure 5I). This result shows that in the case of the chronological lifespan phenotype, *agm1* is epistatic of *tco89*. In addition, while *tco89* negatively interacts with *agm1*, the effect on anabolism and growth is profound but does not reflect, in this case, to the ageing phenotype. Our data reveal that the agmatinergic branch of arginine catabolism is favoured during mTOR inhibition and forms a regulatory loop required for maintaining lower mTOR level, according to what environmental pressures dictate (Figure 5J).

Discussion

In this study we have assessed the cellular and molecular effects of rapalink-1 using fission yeast, a genetically tractable eukaryotic model. Our results show that rapalink-1 targets TORC1, prolongs chronological ageing and demonstrate that mTOR activity negatively regulates agmatinase genes. In fast

growing conditions and nutrient availability, mTOR is highly active. The cells retain mTOR activity, thus, enhancing anabolism and promoting growth and, therefore, repress agmatinase genes and the catabolic processing of arginine pools. This metabolic circuit ensures that arginine, stored within vacuoles (Mülleder et al., 2016), continues to activate mTOR. In stress conditions (including stationary phase and during chronological lifespan) and when mTOR activity is lower (López-Maury et al., 2008), cells catabolise arginine. Once again, this ensure that in such conditions cells upregulate defensive mechanisms, scavenge and recycle nutrients and prevent anabolism. Fission yeast arginases Aru1 and Car1 process arginine to ornithine. Interestingly, upon direct TORC1 inhibition through rapalink-1 the main arginase Aru1 is downregulated while Car1 is upregulated 1.4-fold. Data from the orfeome and global localisation study (Matsuyama et al., 2006) indicate that Aru1 and Car1 are found in the cytoplasm and the nucleus. Nevertheless, agm1 and agm3 (there are no relevant data on agm2) are found in the endoplasmic reticulum (reticulophagy is a GO for genes intercating with agm1) and the vacuole. Therefore, agmatinase genes are localised in the right compartment to control arginine pools crucial for TORC1 activity and fission yeast cells' survival during stresses and lifespan. Taken together, these data and circuits can explain the requirements of the agmatinases in chronological ageing.

Our gene expression analyses have revealed many TORC-1-regulated genes with no annotations or characterisation related to ageing and lifespan. Recent studies have focused on broad profiling of fission yeast mutants (Rodríguez-López et al., 2023) using non-competitive settings. In addition we and others have performed genome-wide assays (Legon and Rallis, 2022) towards characterising mutants related to lifespan regulation (Romila et al., 2021; Sideri et al., 2015). Despite these efforts and due to the competitive nature of pooled barcode-based assays, only a fraction of the available viable mutants have been characterised. In addition, many medium-or high-throughput lifespan approaches have already been described and conducted in fission yeast (Kamrad et al., 2020; Rallis et al., 2014; Romila et al., 2021). Nevertheless, this gap of knowledge remains and forms a current and future within the biogerontology field and beyond.

Parallel to gene expression analyses we have performed cell-based genome-wide screens to reveal mutants that are sensitive and resistant to rapalink-1 as we have previously reported for torin1 (Rodríguez-López et al., 2020). We have concluded that Pik3 is required, at least partially, for healthspan and lifespan extension resulting from rapalink-1-mediated mTOR inhibition during cell proliferation. Rapalink-1 prolongs lifespan considerably without Pik3, as previously observed for gaf1 and torin1 (Rodríguez-López et

al., 2020). This is anticipated due to the plethora of proteins and compensation mechanisms that might operate downstream of mTOR (see next RNA-seq analysis below) including factors related for endolysosomal processes. Our data showcase that beneficial effects of mTOR inhibition in lifespan are related to this pathway and involve ESCRT, HOPS, CORVET, autophagy and the PIK3 complex. Taken together, these results indicate that these complexes, as in the case of rapalink-1, may be required for mTOR-dependent lifespan control through other inhibitors including rapamycin and torin1. Recent work has linked the inhibition of S6K with lifespan increase through the endolysosomal system (Zhang et al., 2024) showcasing the universal roles of these connections in ageing.

Interest in agmatine as a nutraceutical is significant and it is reported as a promising therapeutic agent for treating a broad spectrum of central nervous system-associated diseases (Akasaka and Fujiwara, 2020). Large portion of agmatine in mammals is supplemented from diets and gut microbiota and long-term (5 years) supplementation studies (Gilad and Gilad, 2014) have demonstrated its safety in the examined doses. Beneficial effects on the host's lifespan through microbiome-derived agmatine induced by metformin treatment have been previously reported (Pryor et al., 2019; Tassoulas and Wackett, 2024). Indeed, agmatine can augment metformin's therapeutic effects. However, it does not always promote beneficial effects as it can contribute to pathology (Yun et al., 2024). Here we show that a consequence of direct TORC1 inhibition is the transcriptional activation of all the enzymes that catabolise agmatine to putrescine and urea with this pathway being vital for viability in non-dividing states. We have performed genome-wide phenomic screens revealing mutant backgrounds that benefit (or not) from agmatine and putrescine treatments. Our results show that supplementations of agmatine and putrescine are beneficial for cellular fitness only when arginine metabolism pathways are intact. This may explain diverse outcomes of agmatine supplementation and possible contributions to pathological conditions that are observed in other studies.

Finally, our analyses reveal a metabolic feedback loop mediated through agmatinase enzymes ensuring that mTORC1 activity levels are maintained as required for physiological cell needs and according to received signals from environmental or pharmacological changes. This metabolic control is required for survival in non-dividing states and chronological lifespan. These results from fission yeast may have implications for human cells in both dividing and non-dividing states. Understanding how mTORC1 activity

is tuned may be beneficial in both normal ageing and also pathological states as well as in cancer where mTOR plays important roles (Laplante and Sabatini, 2012; Marques-Ramos and Cervantes, 2023).

Methods

Strains and Media

972 h− was used as the *wild-type*. The strain containing C-terminally GFP-tagged Gaf1 (*gaf1-GFP kanMX6*) has been generated according to (Bähler et al., 1998) with *gaf1* being under the control of the endogenous promoter and as in (Rallis et al., 2021, 2017; Rodríguez-López et al., 2020). Strains Maf-1-pK and GFP-atg8 have been previously described (Davie et al., 2015; Mukaiyama et al., 2010). We have also used *h+ agm1::kanMX6; h+ agm2::kanMX6; h+ agm3::kanMX6; h+ fkh1::kanMX6; h+ pik3::kanMX6; agm1::natMX6 agm3::kanMX6; agm1::natMX6 tco89::kanMX6* (Kim et al., 2010). Microscopy was performed using an EVOS M5000 and Leica DMRA2 epi-fluorescent microscope fitted with a monochrome Orca-ER camera from Hamamatsu Photonics. YES and EMM2 media (Formedium) are used as indicated in figures and main text. Drug treatments have been conducted in fast growing cultures at OD_{600} 0.5 (see main text for details). Liquid cultures were grown at 32°C with shaking at 130 rpm.

Western blotting

Cells were treated with 100 nM rapamycin or 100 nM rapalink-1 for two or five hours as indicated in figures and main text. Cells were disrupted using RIPA buffer and glass beads in a FastPrep 5G MP lysis system. Antibodies directed against phospho-eIF2a (#9721, 1:1,000), eIF2a (#9722, 1:1,000), phospho-Ssp2 (#50081, 1:1,000), Phospho-(Ser/Thr) Akt Substrate Antibody (#9611, 1:2,000) were purchased from Cell Signaling Technologies. The antibodies directed against V5 (sc-81594, 1:1,000) and HA (sc-7392, 1:1,000) were purchased from Santa Cruz Biotechnology. Secondary antibodies Goat Anti-Mouse IgG H&L (HRP) (ab205719) and Goat Anti-Rabbit IgG H&L (HRP) (ab205718) were purchased from Abcam while the ECL Western Blotting Detection system was from Pierce™. □-tubulin (T5168, 1:1,000) and anti-GFP (11814460001, 1:1,000) were purchased from Sigma-Aldrich. □-tubulin and Ponceau S staining have been used as loading controls for western blots as and where indicated. Western blotting quantifications have been performed using ImageJ/Fiji (Schindelin et al., 2012) as previously described (Rallis et al., 2014).

Cell size and septation index determination

To measure septation index, cells were resuspended in calcofluor solution (18909, Sigma-Aldrich) and incubated at room temperature for five minutes. Cells were visualized using an EVOS M5000 microscope. Percentages of septation from 200 cells for each time point have been recorded. For cell length at division, measurements of 50-100 septated cells were conducted using Fiji/ImageJ software (Schindelin et al., 2012) as previously described (Rallis et al., 2017).

Chronological Lifespan (CLS) Assays

CLS was determined as previously described in (Rallis et al., 2013). Fission yeast cells are grown to stationary phase. However, in this study, cells are left for an additional 48 hours as seen in previous related studies (Roux et al., 2009) and then the assay starts with this time point considered as the 100% survival for the time course. 2 or 3 independent biological repeats with each repeat having 3 technical replicates have been used. Log rank tests are performed for all CLS assays with CFUs and percentages used in the statistical testing. Statistical significance has been also validated with AUC measurements (Schindelin et al., 2012) as previously described in (Rodríguez-López et al., 2020) and where indicated/shown. Lifespan lengths vary largely in yeasts depending on the time point used following stationary phase entry and the media used. Different batches of YES media can generate different lifespan curve patterns depending on the Yeast Extract used in the particular batch. We have used a unique YES batch (Formedium) throughout the study.

RNA Sequencing data

Untreated as well as rapamycin and rapalink-1 treated cells (treatment was at OD_{600}=0.5) for 5 hrs were harvested and processed for RNA isolation as previously described (ref) using acidic phenol-chloroform extraction method followed by RNAeasy (Qiagen) cleanup with on column DNase treatments before double elution. Followign appropriate quality control steps, RNA library formed by polyA capture and Illumina 150 bp paired-end sequencing followed by standard R-based bioinformatic analysis was performed. Differential gene expression analysis of two conditions/groups (two biological replicates per condition) was performed using DESeq2R package (1.20.0). Genes with an adjusted P-value <=0.05 found by DESeq2 and at various fold cutoffs (see main text) were assigned as differentially expressed. Sequences are deposited at GEO (accession number: GSE2722A).

High throughput phenomics screens

The deletion library (Kim et al., 2010) was arrayed on solid YES media at 1536-spot density, with each strain represented by 4 spots with various concentrations of drugs as indicated for each assay. Plates were incubated at 32°C and high-resolution images of the plates were acquired. Colony size quantitations were then performed using the R package Gitter (Wagih and Parts, 2014). Median colony sizes were calculated for each plate and replicate. Strain colony size data per condition were normalized to the corresponding growth on YES.

Synthetic genetic arrays

SGAs were performed using the Bioneer v5.0 haploid library (Kim et al., 2010) essentially as described previously (Rallis et al., 2017), with each interaction examined in quadruplicate. Query strains were the following: *h− agm1::natMX6*, and control query *h− ade6::natMX6*. Colony size was used as a proxy for double mutant fitness. Colony size measurements were obtained using the gitter package (Wagih and Parts, 2014). Library mutants which fell within 30 kb distance of query mutations were excluded from the respective datasets to avoid spurious interactions as well as mutants for which the *ade6* double mutant colony size was less than 50 pixels as they were deemed to be present in too little amount for accurate interaction values to be calculated. Colony sizes were normalised to the plate median accounting for the effect of the query mutation and plate-specific effects and normalised for column- or row-specific effects. Medians of colony sizes of the SGAs were normalised with respect to the *ade6* SGA (which represents fitness of library single mutants as this query does not affect the library) to calculate the value of genetic interactions between query and library mutants. Interactions with high within-replicate variability were excluded. Finally, the logarithms in base 10 of the interaction were used for interaction scores.

Enrichment analyses of interactions.

Enrichment analyses were performed using Metascape (Zhou et al., 2019). p-values were corrected for multiple tests according to FDR. Enrichment analysis was conducted by comparing lists of interacting genes to all genes in the dataset (Bioneer v5.0 collection strains (Kim et al., 2010)).

Funding

This work was supported by funding to C.R. from the the Biotechnology and Biological Sciences Research Council [Research grant numbers: BB/V006916/1, BB/V006916/2]. C.R. also acknowledges support and funding of the group from the Medical Research Council [Grant number: MR/W001462/1]).

Conflict of Interest

None declared.

Acknowledgments

We thank members of the Rallis Lab Rowshan Islan and John-Patrick Alao for critical reading and valuable comments on the manuscript. We are grateful to the Bahler lab for the use of the Biolector micro-fermentation system used in Fig.2A.

Authors' contributions

Conceptualization, C.R.; Methodology, C.R. Investigation, J.K., C.R., Formal Analysis, C.R., J.K.; Writing, C.R., and J.K.; Funding Acquisition, C.R.; Supervision, C.R.

References

Akasaka N, Fujiwara S. 2020. The therapeutic and nutraceutical potential of agmatine, and its enhanced production using Aspergillus oryzae. *Amino Acids* **52**:181–197. doi:10.1007/s00726-019-02720-7

Bähler J, Wu JQ, Longtine MS, Shah NG, McKenzie A, Steever AB, Wach A, Philippsen P, Pringle JR. 1998. Heterologous modules for efficient and versatile PCR-based gene targeting in Schizosaccharomyces pombe. *Yeast* **14**:943–951. doi:10.1002/(SICI)1097-0061(199807)14:10<943::AID-YEA292>3.0.CO;2-Y

Bjedov I, Partridge L. 2011. A longer and healthier life with TOR down-regulation: genetics and drugs. *Biochem Soc Trans* **39**:460–465. doi:10.1042/BST0390460

Bjedov I, Rallis C. 2020. The Target of Rapamycin Signalling Pathway in Ageing and Lifespan Regulation. *Genes (Basel)* **11**. doi:10.3390/genes11091043

Davie E, Forte GMA, Petersen J. 2015. Nitrogen Regulates AMPK to Control TORC1 Signaling. *Current Biology* **25**:445–454. doi:10.1016/j.cub.2014.12.034

Dudin O, Merlini L, Bendezú FO, Groux R, Vincenzetti V, Martin SG. 2017. A systematic screen for morphological abnormalities during fission yeast sexual reproduction identifies a mechanism of actin aster formation for cell fusion. *PLoS Genet* **13**:e1006721. doi:10.1371/journal.pgen.1006721

Duncan CDS, Rodríguez-López M, Ruis P, Bähler J, Mata J. 2018. General amino acid control in fission yeast is regulated by a nonconserved transcription factor, with functions analogous to Gcn4/Atf4. *Proc Natl Acad Sci U S A* **115**:E1829–E1838. doi:10.1073/pnas.1713991115

Fan Q, Aksoy O, Wong RA, Ilkhanizadeh S, Novotny CJ, Gustafson WC, Truong AY-Q, Cayanan G, Simonds EF, Haas-Kogan D, Phillips JJ, Nicolaides T, Okaniwa M, Shokat KM, Weiss WA. 2017. A Kinase Inhibitor Targeted to mTORC1 Drives Regression in Glioblastoma. *Cancer Cell* **31**:424–435. doi:10.1016/j.ccell.2017.01.014

Gilad GM, Gilad VH. 2014. Long-term (5 years), high daily dosage of dietary agmatine--evidence of safety: a case report. *J Med Food* **17**:1256–1259. doi:10.1089/jmf.2014.0026

Gilleron J, Gerdes JM, Zeigerer A. 2019. Metabolic regulation through the endosomal system. *Traffic* **20**:552–570. doi:10.1111/tra.12670

Gonzalez S, Rallis C. 2017. The TOR Signaling Pathway in Spatial and Temporal Control of Cell Size and Growth. *Frontiers in Cell and Developmental Biology* **5**. doi:10.3389/fcell.2017.00061

Harrison DE, Strong R, Sharp ZD, Nelson JF, Astle CM, Flurkey K, Nadon NL, Wilkinson JE, Frenkel K, Carter CS, Pahor M, Javors MA, Fernandez E, Miller RA. 2009. Rapamycin fed late in life extends lifespan in genetically heterogeneous mice. *Nature* **460**:392–395. doi:10.1038/nature08221

Hayles J, Wood V, Jeffery L, Hoe K-L, Kim D-U, Park H-O, Salas-Pino S, Heichinger C, Nurse P. 2013. A genome-wide resource of cell cycle and cell shape genes of fission yeast. *Open Biol* **3**:130053. doi:10.1098/rsob.130053

Ikai N, Nakazawa N, Hayashi T, Yanagida M. 2011. The reverse, but coordinated, roles of Tor2 (TORC1) and Tor1 (TORC2) kinases for growth, cell cycle and separase-mediated mitosis in Schizosaccharomyces pombe. *Open Biol* **1**:110007. doi:10.1098/rsob.110007

Kamrad S, Rodríguez-López M, Cotobal C, Correia-Melo C, Ralser M, Bähler J. 2020. Pyphe, a python toolbox for assessing microbial growth and cell viability in high-throughput colony screens. *Elife* **9**. doi:10.7554/eLife.55160

Kim D-U, Hayles J, Kim D, Wood V, Park H-O, Won M, Yoo H-S, Duhig T, Nam M, Palmer G, Han S, Jeffery L, Baek S-T, Lee H, Shim YS, Lee M, Kim L, Heo K-S, Noh EJ, Lee A-R, Jang Y-J, Chung K-S, Choi S-J, Park J-Y, Park Y, Kim HM, Park S-K, Park H-J, Kang E-J, Kim HB, Kang H-S, Park H-M, Kim K, Song K, Song KB, Nurse P, Hoe K-L. 2010. Analysis of a genome-wide set of gene deletions in the fission yeast Schizosaccharomyces pombe. *Nat Biotechnol* **28**:617–623. doi:10.1038/nbt.1628

Kuroshima K, Yoshino H, Okamura S, Tsuruda M, Osako Y, Sakaguchi T, Sugita S, Tatarano S, Nakagawa M, Enokida H. 2020. Potential new therapy of Rapalink-1, a new generation mammalian target of rapamycin inhibitor, against sunitinib-resistant renal cell carcinoma. *Cancer Sci* **111**:1607–1618. doi:10.1111/cas.14395

Laplante M, Sabatini DM. 2012. mTOR signaling in growth control and disease. *Cell* **149**:274–293. doi:10.1016/j.cell.2012.03.017

Laxman S, Sutter BM, Wu X, Kumar S, Guo X, Trudgian DC, Mirzaei H, Tu BP. 2013. Sulfur amino acids regulate translational capacity and metabolic homeostasis through modulation of tRNA thiolation. *Cell* **154**:416–429. doi:10.1016/j.cell.2013.06.043

Legon L, Rallis C. 2022. Genome-wide screens in yeast models towards understanding chronological lifespan regulation. *Brief Funct Genomics* **21**:4–12. doi:10.1093/bfgp/elab011

Lie S, Banks P, Lawless C, Lydall D, Petersen J. 2018. The contribution of non-essential Schizosaccharomyces pombe genes to fitness in response to altered nutrient supply and target of rapamycin activity. *Open Biol* **8**:180015. doi:10.1098/rsob.180015

Ling NXY, Kaczmarek A, Hoque A, Davie E, Ngoei KRW, Morrison KR, Smiles WJ, Forte GM, Wang T, Lie S, Dite TA, Langendorf CG, Scott JW, Oakhill JS, Petersen J. 2020. mTORC1 directly inhibits AMPK to promote cell proliferation under nutrient stress. *Nat Metab* **2**:41–49. doi:10.1038/s42255-019-0157-1

Lock A, Harris MA, Rutherford K, Hayles J, Wood V. 2020. Community curation in PomBase: enabling fission yeast experts to provide detailed, standardized, sharable annotation from research publications. *Database (Oxford)* **2020**:baaa028. doi:10.1093/database/baaa028

López-Maury L, Marguerat S, Bähler J. 2008. Tuning gene expression to changing environments: from rapid responses to evolutionary adaptation. *Nat Rev Genet* **9**:583–593. doi:10.1038/nrg2398

Marques-Ramos A, Cervantes R. 2023. Expression of mTOR in normal and pathological conditions. *Mol Cancer* **22**:112. doi:10.1186/s12943-023-01820-z

Matsuyama A, Arai R, Yashiroda Y, Shirai A, Kamata A, Sekido S, Kobayashi Y, Hashimoto A, Hamamoto M, Hiraoka Y, Horinouchi S, Yoshida M. 2006. ORFeome cloning and global analysis of protein localization in the fission yeast Schizosaccharomyces pombe. *Nat Biotechnol* **24**:841–847. doi:10.1038/nbt1222

Milosevic K, Stevanovic I, Bozic ID, Milosevic A, Janjic MM, Laketa D, Bjelobaba I, Lavrnja I, Savic D. 2022. Agmatine Mitigates Inflammation-Related Oxidative Stress in BV-2 Cells by Inducing a Pre-Adaptive Response. *Int J Mol Sci* **23**:3561. doi:10.3390/ijms23073561

Mukaiyama H, Nakase M, Nakamura T, Kakinuma Y, Takegawa K. 2010. Autophagy in the fission yeast *Schizosaccharomyces pombe*. *FEBS Letters* **584**:1327–1334. doi:10.1016/j.febslet.2009.12.037

Mülleder M, Calvani E, Alam MT, Wang RK, Eckerstorfer F, Zelezniak A, Ralser M. 2016. Functional Metabolomics Describes the Yeast Biosynthetic Regulome. *Cell* **167**:553-565.e12. doi:10.1016/j.cell.2016.09.007

Noguchi C, Wang L, Shetty M, Mell JC, Sell C, Noguchi E. 2021. Maf1 limits RNA polymerase III-directed transcription to preserve genomic integrity and extend lifespan. *Cell Cycle* **20**:247–255. doi:10.1080/15384101.2021.1874697

Petersen J, Nurse P. 2007. TOR signalling regulates mitotic commitment through the stress MAP kinase pathway and the Polo and Cdc2 kinases. *Nature Cell Biology* **9**:1263–1272. doi:10.1038/ncb1646

Pryor R, Norvaisas P, Marinos G, Best L, Thingholm LB, Quintaneiro LM, De Haes W, Esser D, Waschina S, Lujan C, Smith RL, Scott TA, Martinez-Martinez D, Woodward O, Bryson K, Laudes M, Lieb W, Houtkooper RH, Franke A, Temmerman L, Bjedov I, Cochemé HM, Kaleta C, Cabreiro F. 2019. Host-Microbe-Drug-Nutrient Screen Identifies Bacterial Effectors of Metformin Therapy. *Cell* **178**:1299-1312.e29. doi:10.1016/j.cell.2019.08.003

Rallis C, Codlin S, Bähler J. 2013. TORC1 signaling inhibition by rapamycin and caffeine affect lifespan, global gene expression, and cell proliferation of fission yeast. *Aging Cell* **12**:563–573. doi:10.1111/acel.12080

Rallis C, López-Maury L, Georgescu T, Pancaldi V, Bähler J. 2014. Systematic screen for mutants resistant to TORC1 inhibition in fission yeast reveals genes involved in cellular ageing and growth. *Biol Open* **3**:161–171. doi:10.1242/bio.20147245

Rallis C, Mülleder M, Smith G, Au YZ, Ralser M, Bähler J. 2021. Amino Acids Whose Intracellular Levels Change Most During Aging Alter Chronological Life Span of Fission Yeast. *J Gerontol A Biol Sci Med Sci* **76**:205–210. doi:10.1093/gerona/glaa246

Rallis C, Townsend S, Bähler J. 2017. Genetic interactions and functional analyses of the fission yeast gsk3 and amk2 single and double mutants defective in TORC1-dependent processes. *Sci Rep* **7**:44257. doi:10.1038/srep44257

Rodríguez-López M, Bordin N, Lees J, Scholes H, Hassan S, Saintain Q, Kamrad S, Orengo C, Bähler J. 2023. Broad functional profiling of fission yeast proteins using phenomics and machine learning. *Elife* **12**:RP88229. doi:10.7554/eLife.88229

Rodríguez-López M, Gonzalez S, Hillson O, Tunnacliffe E, Codlin S, Tallada VA, Bähler J, Rallis C. 2020. The GATA Transcription Factor Gaf1 Represses tRNAs, Inhibits Growth, and Extends Chronological Lifespan Downstream of Fission Yeast TORC1. *Cell Rep* **30**:3240-3249.e4. doi:10.1016/j.celrep.2020.02.058

Romila CA, Townsend S, Malecki M, Kamrad S, Rodríguez-López M, Hillson O, Cotobal C, Ralser M, Bähler J. 2021. Barcode sequencing and a high-throughput assay for chronological lifespan uncover ageing-associated genes in fission yeast. *Microb Cell* **8**:146–160. doi:10.15698/mic2021.07.754

Roux AE, Arseneault G, Chartrand P, Ferbeyre G, Rokeach LA. 2010. A screen for genes involved in respiration control and longevity in Schizosaccharomyces pombe. *Ann N Y Acad Sci* **1197**:19–27. doi:10.1111/j.1749-6632.2010.05198.x

Roux AE, Leroux A, Alaamery MA, Hoffman CS, Chartrand P, Ferbeyre G, Rokeach LA. 2009. Pro-aging effects of glucose signaling through a G protein-coupled glucose receptor in fission yeast. *PLoS Genet* **5**:e1000408. doi:10.1371/journal.pgen.1000408

Rutherford KM, Lera-Ramírez M, Wood V. 2024. PomBase: a Global Core Biodata Resource-growth, collaboration, and sustainability. *Genetics* **227**:iyae007. doi:10.1093/genetics/iyae007

Schindelin J, Arganda-Carreras I, Frise E, Kaynig V, Longair M, Pietzsch T, Preibisch S, Rueden C, Saalfeld S, Schmid B, Tinevez J-Y, White DJ, Hartenstein V, Eliceiri K, Tomancak P, Cardona A. 2012. Fiji: an open-source platform for biological-image analysis. *Nature Methods* **9**:676–682. doi:10.1038/nmeth.2019

Schmeisser K, Parker JA. 2019. Pleiotropic Effects of mTOR and Autophagy During Development and Aging. *Front Cell Dev Biol* **7**:192. doi:10.3389/fcell.2019.00192

Sideri T, Rallis C, Bitton DA, Lages BM, Suo F, Rodríguez-López M, Du L-L, Bähler J. 2015. Parallel Profiling of Fission Yeast Deletion Mutants for Proliferation and for Lifespan During Long-Term Quiescence. *G3* **5**:145–155. doi:10.1534/g3.114.014415

Tassoulas LJ, Wackett LP. 2024. Insights into the action of the pharmaceutical metformin: Targeted inhibition of the gut microbial enzyme agmatinase. *iScience* **27**:108900. doi:10.1016/j.isci.2024.108900

Thoreen CC, Kang SA, Chang JW, Liu Q, Zhang J, Gao Y, Reichling LJ, Sim T, Sabatini DM, Gray NS. 2009. An ATP-competitive mammalian target of rapamycin inhibitor reveals rapamycin-resistant functions of mTORC1. *J Biol Chem* **284**:8023–8032. doi:10.1074/jbc.M900301200

Thoreen CC, Sabatini DM. 2009. Rapamycin inhibits mTORC1, but not completely. *Autophagy* **5**:725–726. doi:10.4161/auto.5.5.8504

Valbuena N, Guan K-L, Moreno S. 2012a. The Vam6 and Gtr1-Gtr2 pathway activates TORC1 in response to amino acids in fission yeast. *J Cell Sci* **125**:1920–1928. doi:10.1242/jcs.094219

Valbuena N, Rozalén AE, Moreno S. 2012b. Fission yeast TORC1 prevents eIF2α phosphorylation in response to nitrogen and amino acids via Gcn2 kinase. *J Cell Sci* **125**:5955–5959. doi:10.1242/jcs.105395

Wagih O, Parts L. 2014. gitter: A Robust and Accurate Method for Quantification of Colony Sizes From Plate Images. *G3 Genes|Genomes|Genetics* **4**:547–552. doi:10.1534/g3.113.009431

Yun C, Yan S, Liao B, Ding Y, Qi X, Zhao M, Wang K, Zhuo Y, Nie Q, Ye C, Xia P, Ma M, Li R, Jiang C, Qiao J, Pang Y. 2024. The microbial metabolite agmatine acts as an FXR agonist to promote polycystic ovary syndrome in female mice. *Nat Metab* **6**:947–962. doi:10.1038/s42255-024-01041-8

Zhang P, Catterson JH, Grönke S, Partridge L. 2024. Inhibition of S6K lowers age-related inflammation and increases lifespan through the endolysosomal system. *Nat Aging* **4**:491–509. doi:10.1038/s43587-024-00578-3

Zhou H, Li X, Rana M, Cornelius JF, Khan D, Muhammad S. 2023. mTOR Inhibitor Rapalink-1 Prevents Ethanol-Induced Senescence in Endothelial Cells. *Cells* **12**:2609. doi:10.3390/cells12222609

Zhou Y, Zhou B, Pache L, Chang M, Khodabakhshi AH, Tanaseichuk O, Benner C, Chanda SK. 2019. Metascape provides a biologist-oriented resource for the analysis of systems-level datasets. *Nat Commun* **10**:1523. doi:10.1038/s41467-019-09234-6

Figure 1 (Kumar and Rallis)

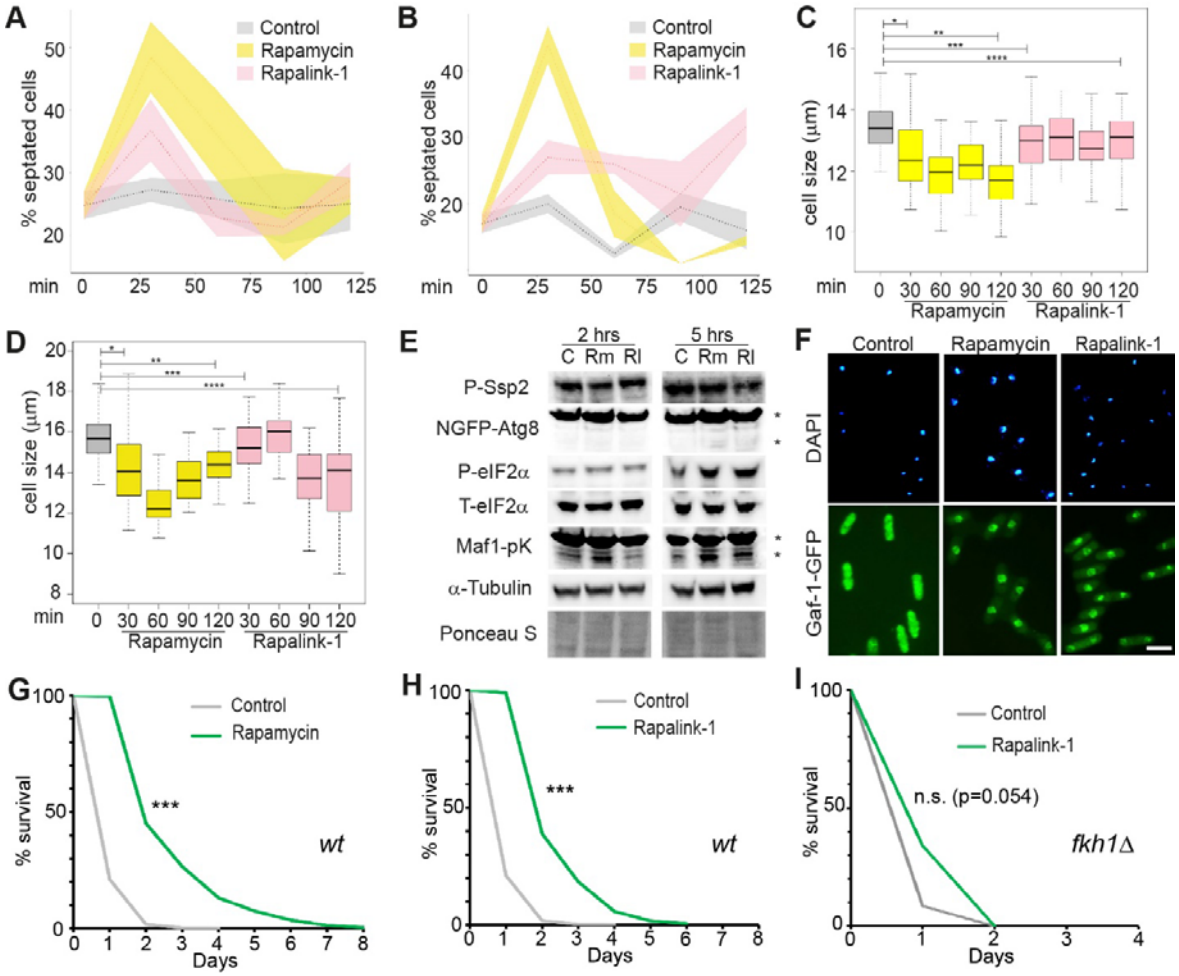

Rapalink-1 affects TORC1-related processes in fission yeast and prolongs lifespan.

(A) Time course of septation index for untreated (control) and rapamycin and rapalink-1 treated cells (100 nM), as indicated, in YES media. Dotted lines represent average values while coloured ribbons standard deviation from three independent counts.

(B) Same as in A in EMM2 minimal media.

(C) Time course of cell size upon division measurements following rapamycin and rapalink-1 treatments in YES media. Asterisks indicate statistically significant differences between the compared groups ($p<0.01$, wilcoxon testing).

(D) Same as described in panel C with the assay conducted in EMM2 media.

(E) Western blots for markers dependent on TORC1 activity and representative loading controls. Assays

have been conducted following 2 hrs and 5 hrs of treatments with 100 nM rapamycin (Rm) and rapalink-1 (Rl) together with untreated control cells (C).

(F) DAPI staining and Gaf1-GFP localisation panels in control untreated, rapamycin and rapalink-1 treated cells as indicated.

(G) CLS assays for untreated (control) and rapamycin treated wild-type fission yeast cells (log-rank $p=1.25*10^{-12}$, see materials and methods).

(H) CLS assays for untreated (control) and rapalink-1 treated wild-type fission yeast cells (log-rank $p=2.2*10^{-12}$, see materials and methods).

(I) CLS assays for untreated (control) and rapalink-1 treated *fkh1Δ* mutant cells (log-rank p=0.047, see materials and methods).

*** in lifespans indicate p values <0.001.

Figure 2 (Kumar and Rallis)

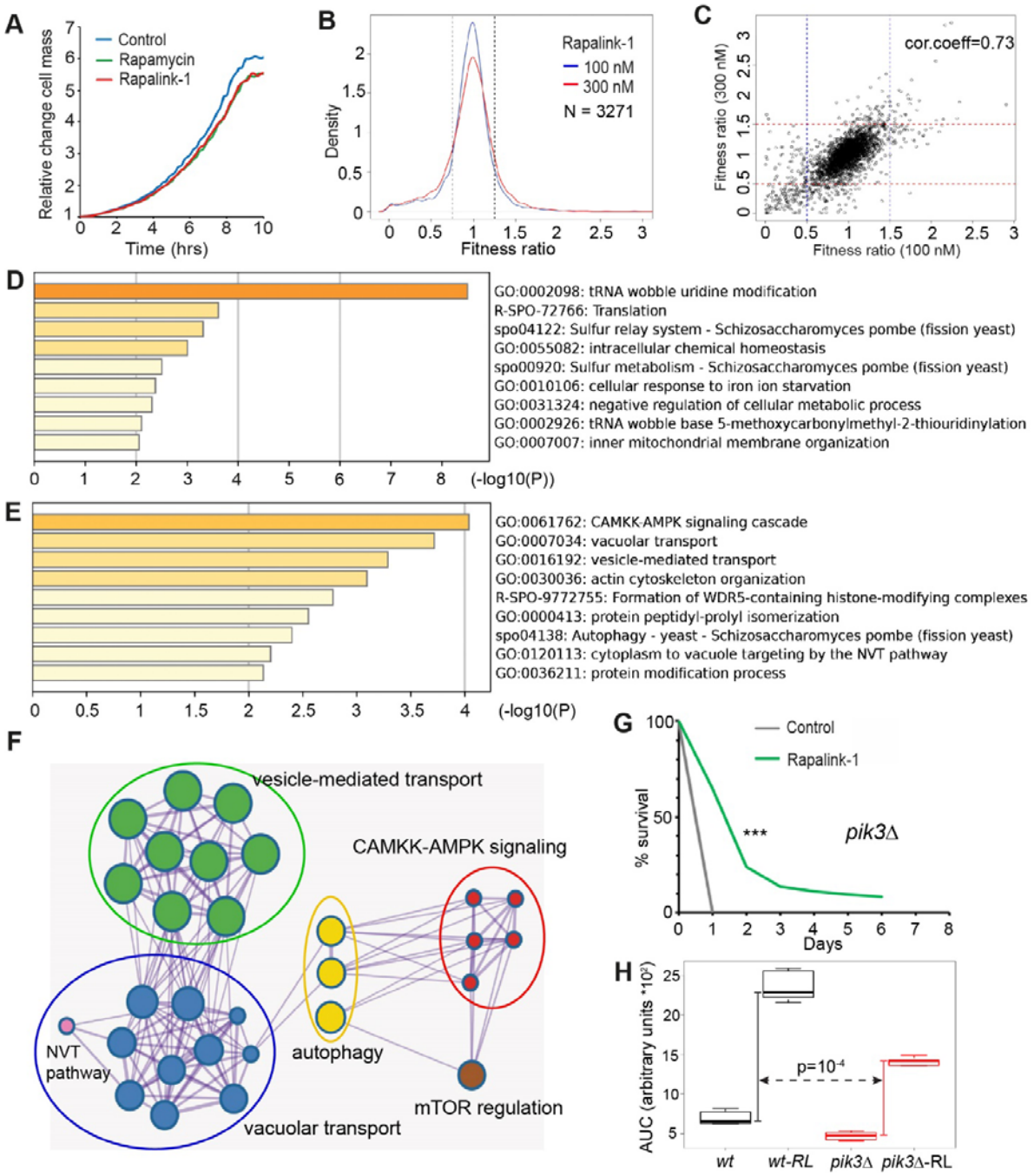

2

A genome-wide screen for rapalink-1 points to the endosome-vacuole-lysosome network as important in mTOR-dependent lifespan regulation.

(A) Growth curves for control untreated, rapamycin and rapalink-1 treated wild type fission yeast cells, as indicated. The assay records light scattering dependent on culture cell mass (see materials and methods).

(B) Fitness ratio overviews of genome-wide screens (data acquired for 3,271 deletion mutants) for rapalink-1 at the indicated concentrations. Vertical dotted lines indicate cutoffs for sensitive and resistant mutants (Supplementary table 1).

(C) Fitness ratio correlation between the two conducted screens. Each point represents the average fitness obtained for a single deletion mutant of the library.

(D) Gene ontology enrichment for mutants sensitive to rapalink-1 treatment.

(E) Gene ontology enrichment for mutants resistant to rapalink-1 treatment.

(F) Network of enriched terms colored by cluster ID, where nodes that share the same cluster ID are typically close to each other.

(G) CLS assay for untreated and rapalink-1 treated *pik3Δ* cells as indicated (log rank $p=10^{-5}$).

(H) AUC for lifespan assays of *wt* and *pik3Δ* mutant cells without or with rapalink-1 treatment (*wt-RL* and *pik3Δ-RL* respectively. Vertical bars: rapalink-1-mediated increase in average AUC values for *wt* (black) and *pik3Δ* (red) for curves until day 6 (*wt* curve shown in Fig.1), with the p value reflecting the significantly larger lifespan increase in *wt* than in *pik3Δ* cells.

*** in lifespans indicate p values <0.001.

Figure 3 (Kumar and Rallis)

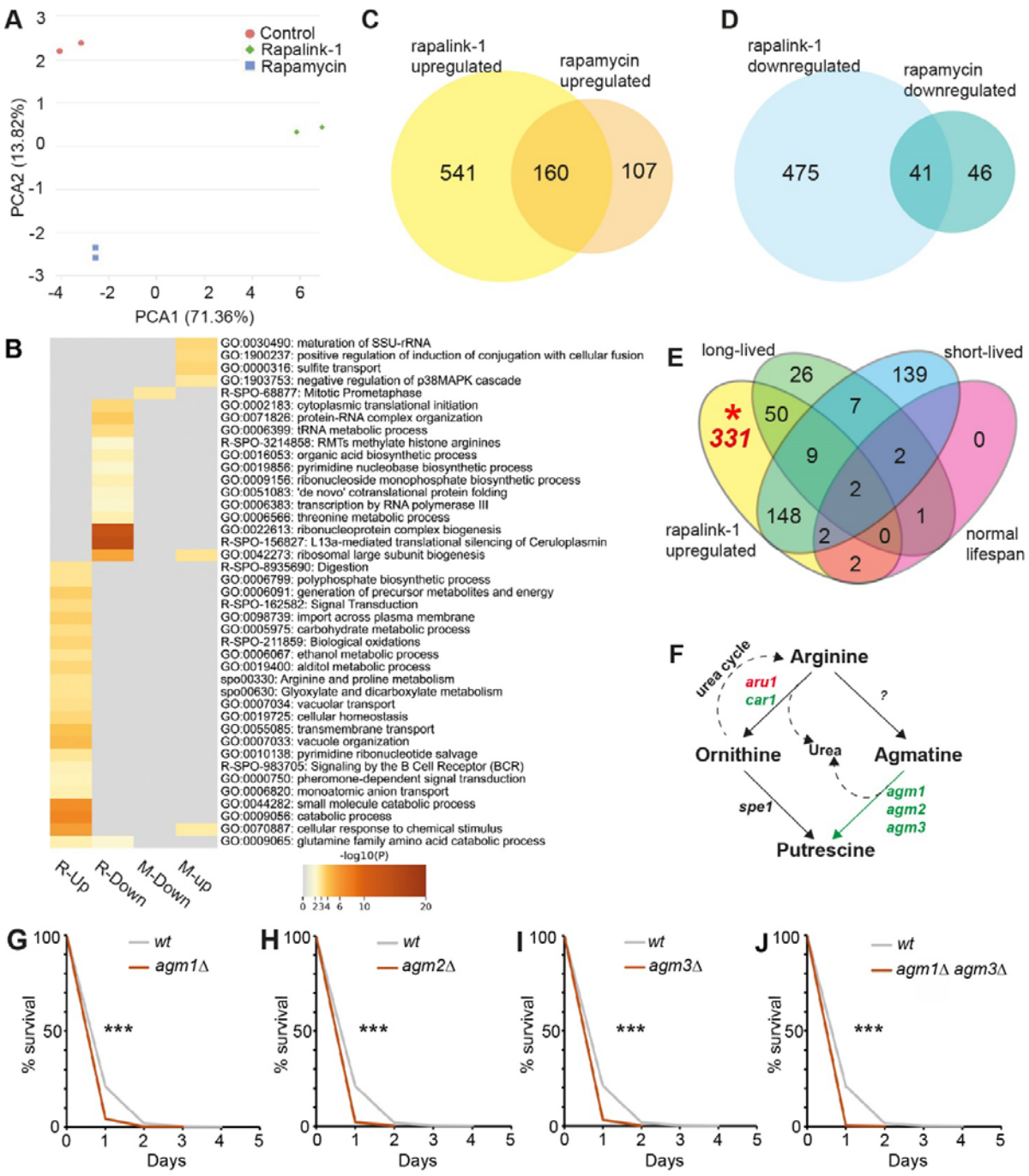

Gene expression analysis following rapamycin and rapalink-1 treatment reveals novel genes involved in chronological ageing.

(A) PCA analysis of control untreated, rapamycin- and rapalink-1-treated cells as indicated.

(B) Heatmap of representative GO enrichments for gene lists of upregulated and downregulated genes in the drug treatments used (R-Up: rapalink-1 upregulated; R-Down: rapalink-1

downregulated; M-up: rapamycin upregulated; M-down: rapamycin downregulated).

(C) Venn diagram for upregulated genes following rapamycin and rapalink-1 treatments.

(D) Venn diagram for downregulated genes following rapamycin and rapalink-1 treatments.

(E) Venn diagram showing overlaps of rapalink-1 upregulated genes (the portion that corresponding mutants are viable) with genes that their deletions lead to long-lived, short-lived or normal-lived mutants.

(F) Schematic of arginine metabolism to ornithine, agmatine and putrescine with genes coding for responsible enzymes. In green: genes that are upregulated, red: downregulated, black: not affected, following rapalink-1 treatment.

(G-J) CLS for normal (*wt*) and mutant *agm1Δ* (G, log rank $p=9.7x10^{-5}$), *agm2Δ* (H, log rank $p=1.5x10^{-5}$), *agm3Δ* (I, log rank, $p=3.9x10^{-5}$), and *agm1Δ agm3Δ* (J, log rank $p=3.3x10^{-6}$) cells as indicated.

*** in lifespans indicate p values <0.001.

Supplemental Figure 1 (Kumar and Rallis)

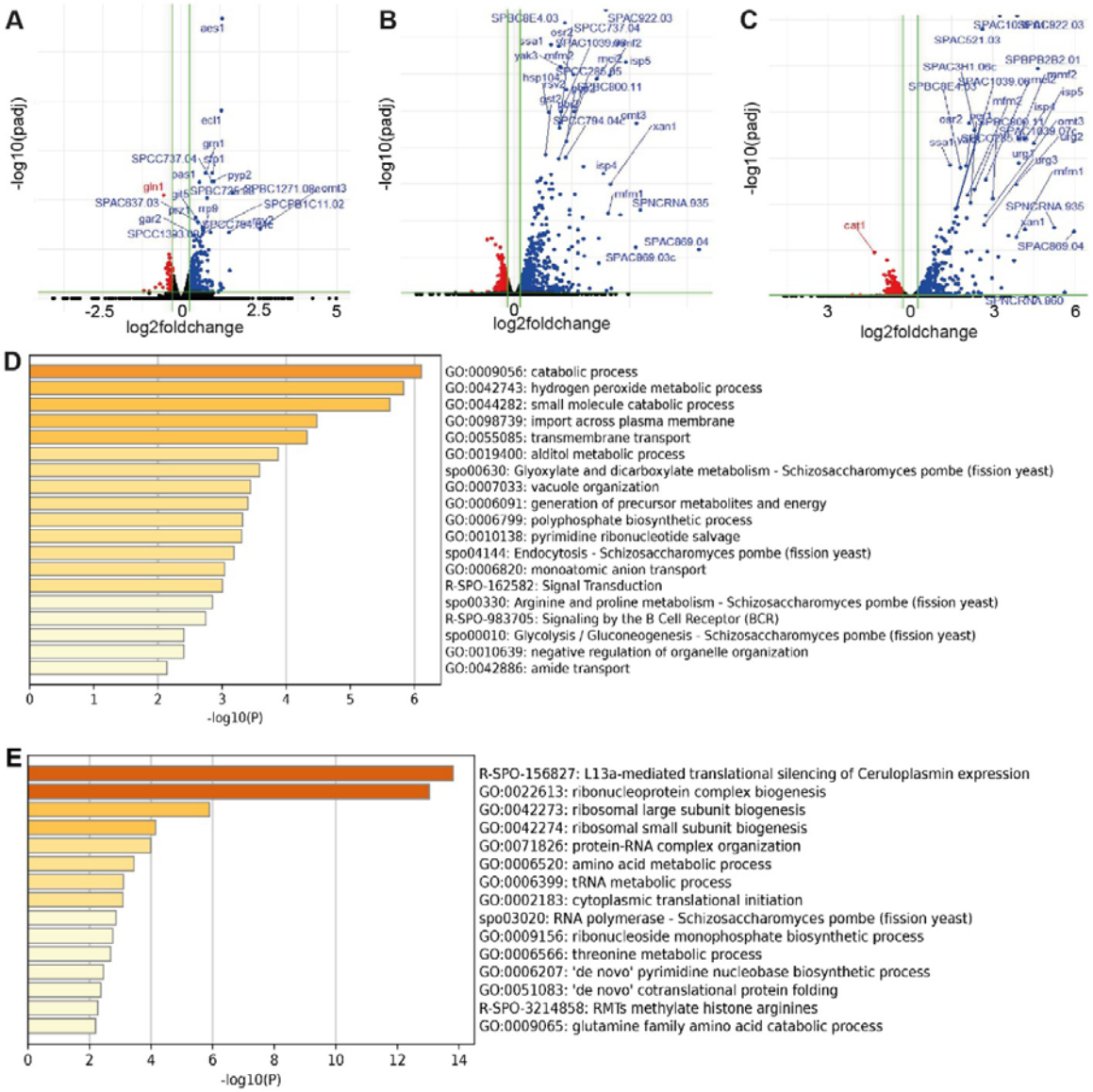

RNAseq data analyses of the paper related to Figure 3.

(A-C) Volcano plots with upregulated (red), downregulated (blue) and unchanged (black) genes.

(A) Untreated versus rapamycin-treated cells.

(B) Untreated versus rapalink-1-treated cells.

(C) rapamycin versus rapalink-1-treated cells.

(D) Bar graph representation of representative GO ontology enrichments for genes upregulated in rapalink-1 treatment only (related to Figure 3E)

(E) Bar graph representation of representative GO ontology enrichments for genes downregulated in

rapalink-1 treatment only (related to Figure 3F).

Supplemental Figure 2 (Kumar and Rallis)

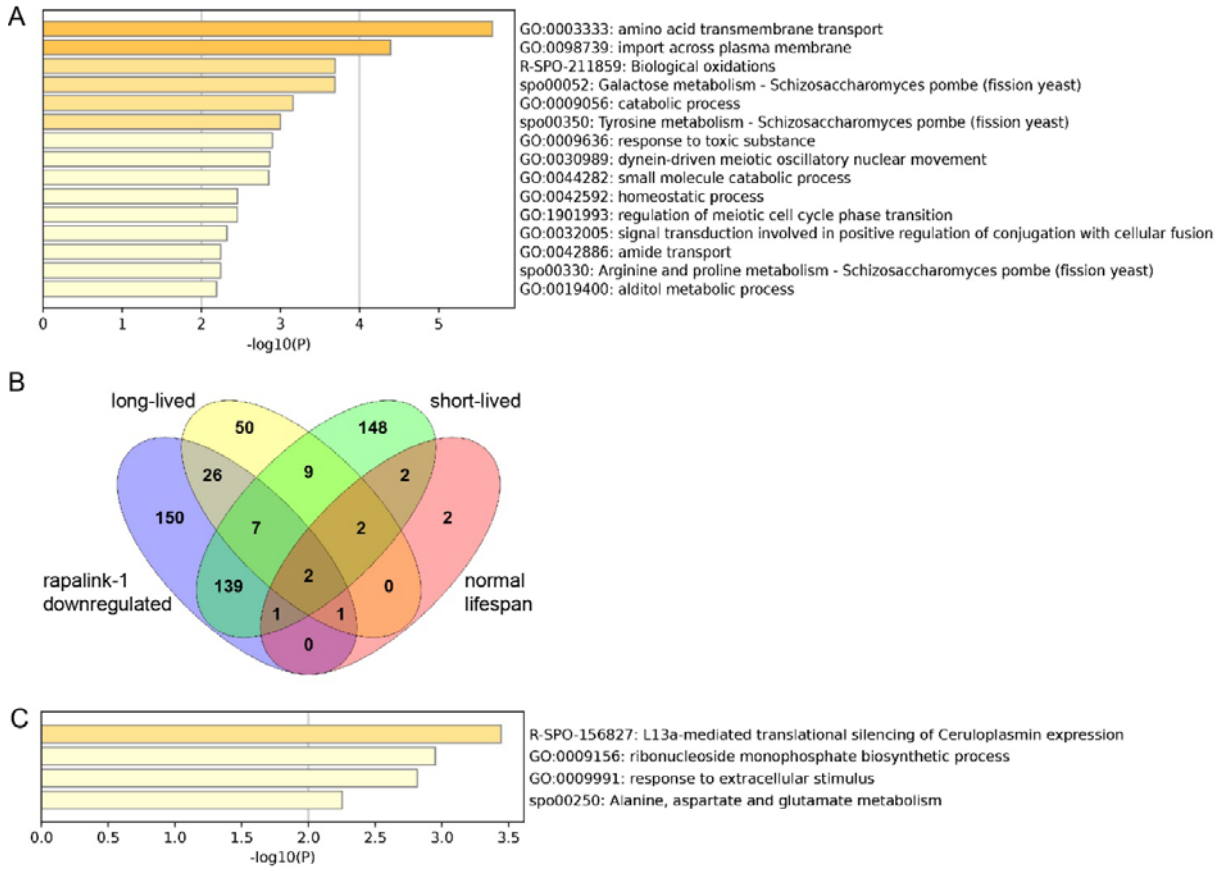

Gene expression analyses and enrichments related to rapalink-1.

(A) Bar graph schematic for representative GO ontology enrichments of rapalink-1-upregulated genes not related to lifespan phenotype (related to Figure 2H, genes in red fonts).

(B) Venn diagram showing overlaps of rapalink-1 downregulated genes (the portion that corresponding mutants are viable) with genes that their deletions lead to long-lived, short-lived or normal-lived mutants.

(C) Bar graph schematic for representative GO ontology enrichments of the 150 rapalink-1-downregulated genes not related to lifespan phenotype shown in (B).

Figure 4 (Kumar and Rallis)

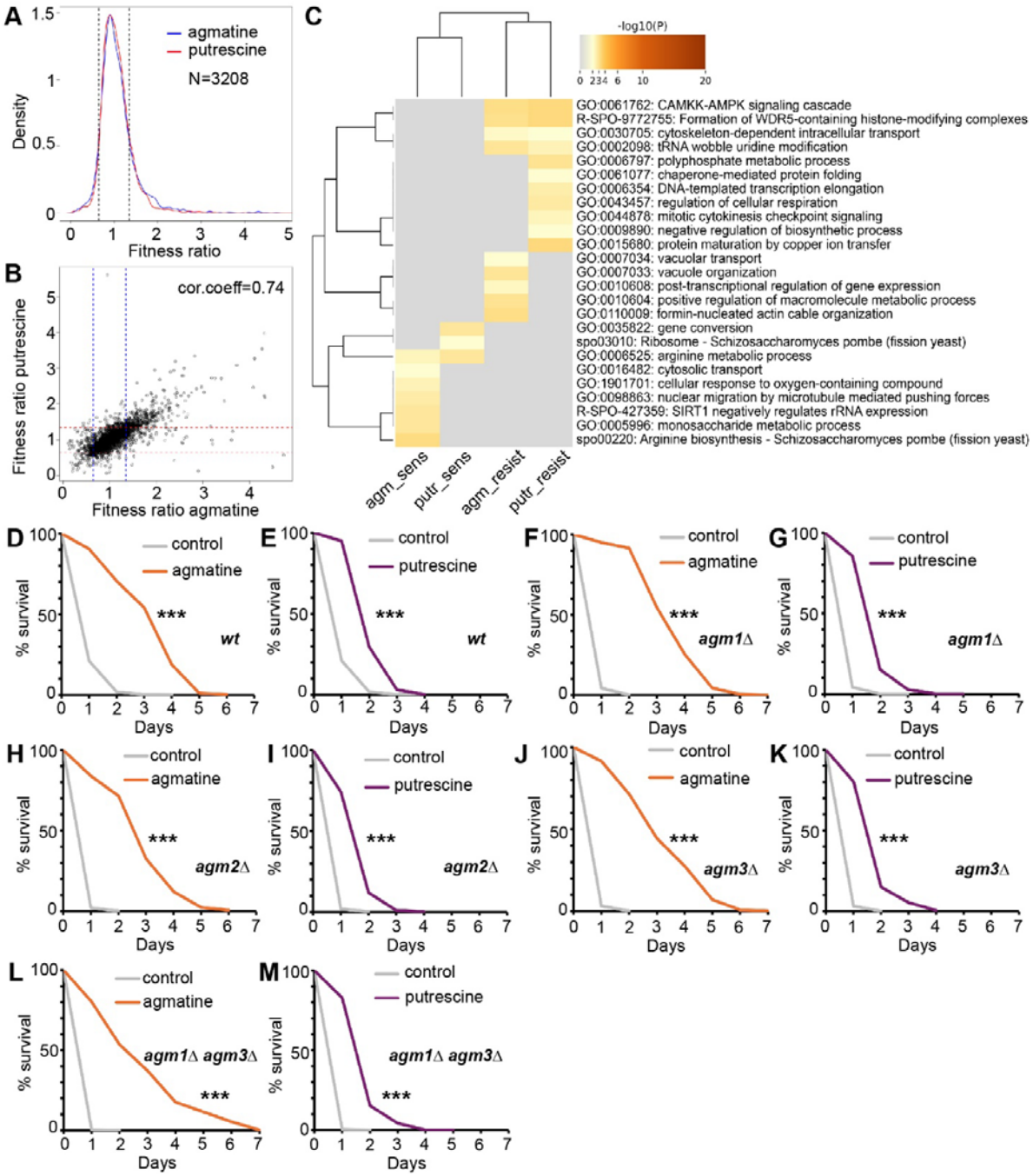

Genome-wide fitness screens of agmatine and putrescine and effects on chronological lifespan of fission yeast.

(A) Density profiles of fitness ratios for 3,208 *S. pombe* deletion mutants following agmatine and putrescine treatments.

(B) Correlation of fitness ratios of deletion mutants in agmatine and putrescine screens. Each point

represents the average fitness value for each mutant.

(C) Heatmap of representative Gene Ontology enrichments for mutant strains resistant and sensitive to drug treatments (agm_sens: sensitive to agmatine; putr_sens: sensitive to putrescine; agm_resist: resistant to agmatine; putr_resist: resistant to putrescine).

(D-M) CLS for normal (*wt*) and agmatinase mutant cells following agmatine and putrescine supplementation during growth phase (see material and methods) as indicated.

*** in lifespans indicate p values <0.001, see log rank p values in the main text.

Figure 5 (Kumar and Rallis)

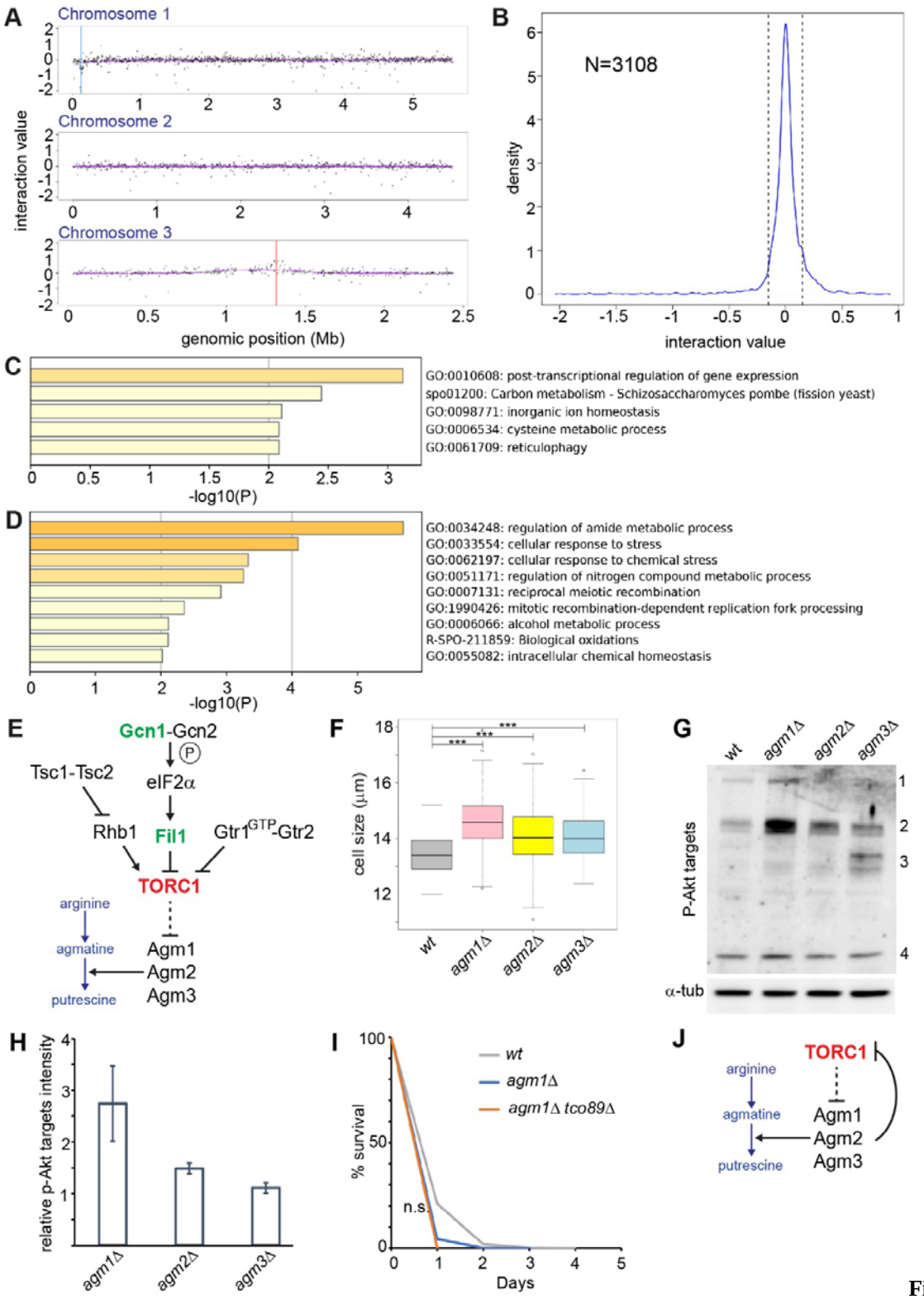

781 **Figure 5**

782 **Genetic interactomes of *agm1* reveal a metabolic feedback mechanism that tunes mTORC1 activity.**

783 (A) Physical mapping of *agm1* interaction values with 3,108 mutants.

(B) Density plot of the genome-wide *agm1* genetic interactions. Vertical dotted lines show the cutoffs set for the interactome analysis (see materials and methods).

(C) Bar graph representation of GO enrichments for negative *agm1* interactions.

(D) Bar graph representation of GO enrichments for positive *agm1* interactions.

(E) Schematic showing a previously reported tripartite mTORC1 regulation in fission yeast. Green fonts signify positive while red fonts negative interactions.

(F) Cell size upon division measurements in normal (wt) and *agm* mutant cells (*agm1Δ, agm2Δ, agm3*Δ) in YES media. Asterisks indicate statistically significant differences between the compared groups ($p<0.01$, wilcoxon testing).

(G) Western blot for p-Akt targets in normal (wt) and *agm* mutant cells (*agm1Δ, agm2Δ, agm3*Δ) with accompanied α-tubulin western blot as loading control. Side numbers (1-4) indicate various detected targets. No 4 represents and used in literature (Ling et al., 2020) for pRps6.

(H) Quantification of -Akt target signal (whole lane) from two repeats of the blot shown in (G).

(I) CLS patterns of *agm1Δ and agm1Δ tco89Δ* mutants is indicated. N.s.: log rank $p>0.05$

(J) A schematic model for the revealed role of agmatinase enzymes in tuning mTORC1 activity in fission yeast.

SUPPLEMENTAL TABLES

Supplementary Table 1

List of rapalink-1 sensitive (<0.75, representing 25% smaller colony compared to untreated control) and resistant (>1.25, 25% larger colony compared to untreated control) mutant strains.

Supplementary Table 2

List of genes upregulated in fast growing fission yeast cells (0.5 OD_{600}) following 5 hrs of 100nM rapamycin treatment in YES media.

Supplementary Table 3

List of genes downregulated in fast growing fission yeast cells (0.5 OD_{600}) following 5 hrs of 100nM rapamycin treatment in YES media.

Supplementary Table 4

List of genes upregulated in fast growing fission yeast cells (0.5 OD_{600}) following 5 hrs of 100nM rapalink-1 treatment in YES media.

Supplementary Table 5

List of genes downregulated in fast growing fission yeast cells (0.5 OD_{600}) following 5 hrs of 100nM rapalink-1 treatment in YES media.

Supplementary Table 6

Fitness ratio values of mutant strains following genome-wide phenomics screen with Agmatine and Putrescine (see main text and materials and methods).

Supplementary Table 7

Interaction values for all mutant strains against *agm1* following normalisations (see Materials and Methods) and filtering of absent colonies, control and experimental SGA linkage, high variability of colonies and low fitness strains.